Advances in Geosciences
Vol. 30: Planetary Science and Solar & Terrestrial Science (2011)
Ed. Anil Bhardwaj


# INTERACTION OF SOLAR WIND WITH MOON: AN OVERVIEW ON THE RESULTS FROM THE SARA EXPERIMENT ABOARD CHANDRAYAAN-1

ANIL BHARDWAJ* and M. B. DHANYA
*Space Physics Laboratory, Vikram Sarabhai Space Centre, Trivandrum 695022, India*
**anil_bhardwaj@vssc.gov.in; bhardwaj_spl@yahoo.com*

R. SRIDHARAN
*Currently CSIR-ES at Physical Research Laboratory, Ahmedabad, India*

STAS BARABASH, FUTAANA YOSHIFUMI, MARTIN WIESER, MATS HOLMSTRÖM and CHARLES LUE
*Swedish Institute of Space Physics, Box 812, SE-98128 Kiruna, Sweden*

PETER WURZ and AUDREY SCHAUFELBERGER
*Physikalisches Institut, University of Bern, Sidlerstrasse 5, CH-3012 Bern, Switzerland*

KAZUSHI ASAMURA
*Institute of Space and Astronautical Science, 3-1-1 Yoshinodai, Sagamihara, Japan*



The results from the Sub-keV Atom Reflecting Analyzer (SARA) experiment onboard Chandrayaan-1 have revealed several hitherto unknown and interesting aspects about the interaction of solar wind with the Moon. The SARA experiment had two sensors — CENA and SWIM. The Chandrayaan-1 energetic neutrals analyzer (CENA), detected energetic neutral atoms (ENAs), and the Solar Wind Monitor (SWIM) measured ions of solar wind origin. In this review, we summarize the observations made by the SARA experiment, which are: (1) substantial (∼20%) and sustained backscattering of solar wind protons from lunar surface as energetic neutral hydrogen,[1] (2) mini-magnetosphere around magnetic anomalies on Moon using the backscattered ENAs,[2] (3) reflection of solar wind protons from the Moon surface,[3] (4) huge (∼50%) deflection of solar wind protons over strong magnetic anomalies,[4] and (5) presence of protons in the near-lunar plasma wake.[5] These results have implications on the lunar plasma environment, implantation of solar wind hydrogen on lunar surface, and behavior of small scale magnetic anomalies on planetary bodies. The SARA observations suggest that similar processes

may happen on other airless bodies covered with regolith in the solar system as well as in extra-solar system. This paper presents a review of the results obtained from the SARA observation.

## 1. Introduction

The Earth's Moon belongs to a class of planetary bodies which are characterized with a surface bound exosphere[6–9] and lacks a global magnetic field, but has regions of localized crustal magnetic fields referred to as magnetic anomalies.[10–15] The surface of the Moon is covered with a powdered layer called regolith. Solar wind is a magnetized plasma flow from the Sun with a typical composition of around 96% $H^+$, ∼4% $He^{++}$, and <1% heavier ions. The magnetic field lines of the Sun is frozen in to the solar wind plasma and constitutes the interplanetary magnetic field (IMF). Thus, investigation of solar wind interaction with the Moon involves the understanding of particle (plasma) as well as field (magnetic field) interactions.

Due to the very thin atmosphere of the Moon, solar wind particles directly impinges on its surface. It was generally assumed that the solar wind is completely absorbed by the porous regolith[16,17] on the lunar surface. A part of solar wind ions may initiate multiple binary collisions with the lattice atoms on the surface layer which in turn can result in the ejection of a lattice atoms as neutrals or ions with lower energy.[18,19] The energetic neutral atoms (ENAs) being unaffected by electric and magnetic fields travel unobstructed in ballistic trajectories.[20,21] Although theoretical models exist for the sputtering of lunar surface elements,[18] observations were lacking. The continuous bombardment of the solar wind on the Moon surface leads to the change in the surface properties such as surface reflectance of the minerals, a term called space weathering.[22,23] Due to the interaction of solar wind with magnetically anomalous regions, the solar wind may be deflected and a mini-magnetosphere may be formed.[12] Such a system will prevent the solar wind from directly impacting those regions on the lunar surface. Thus, the space weathering of magnetic anomaly regions will be different from that of other regions. This may be reflected in the spectral characteristics of the region at the anomalous region as compared to the surrounding region.

When the solar wind flows past the Moon, it creates a cavity in the downstream which is devoid of plasma and is called the lunar plasma wake. The plasma wake has been observed to close at larger distance (10–20 $R_L$) downstream of the Moon, due to the pressure gradient force between solar

wind plasma and wake.[24,25] Due to the smaller thermal velocity of the protons (∼50 km/s) as compared to the bulk velocity, they are not expected in the near-lunar wake. The counter streaming ion and electron beams are capable of generating instabilities and waves in the wake.[26,27] The more favorable electron access to the nightside lunar surface can results in the negative charging of the Moon surface.[28]

In the recent years, the observations by Kaguya, Chang'E, Chandrayaan-1, IBEX, and ARTEMIS have brought new insight into the neutral and plasma environment of the Moon, localized magnetic field of Moon, and also lunar surface composition. We are now aware that solar wind is not fully absorbed by the Moon surface, but reflected back as ENAs[1,29] as well as ions,[3,30] ion sputtering could be possible on Moon,[31] mini-magnetospheres do exist on the Moon that deflect the impinging solar wind protons[2,32] and protons do enter the near-lunar plasma wake.[5,33–36] All these can change the near-lunar environment significantly.

In this paper we summarize the major findings from the SARA experiment on the Chandrayaan-1 and their comparison with those observed on other recent missions. The implication of these findings for the lunar science and the lunar plasma environment is discussed.



## 2. Instrumentation

The SARA experiment on the Chandrayaan-1, which was a polar orbiting satellite around the Moon, consisted of two sensors — Chandrayaan-1 Energetic Neutrals Analyzer (CENA) and Solar Wind Monitor (SWIM), and a digital processing Unit (DPU). CENA was a neutral particle detector while SWIM was an ion mass analyzer, both of which were capable of doing energy and mass analysis.[20,37–41] The CENA measured neutral particles in the energy range 10–3,000 eV with an energy resolution of 50% and a mass resolution sufficient to distinguish H, O, and heavier species. The SWIM had an energy range 100–15,000 eV with an energy resolution of 7% and a mass resolution sufficient to identify $H^+$, $He^{++}$, $He^+$, and heavier ions. Both the sensors had fan shaped field-of-view (FoV). The total FoV of CENA was 160° × 9° and had seven angular pixels with a resolution of 25° × 9° (FWHM). SWIM had a total FoV of 180° × 7.5° with 16 angular pixels having a resolution of 10° × 7.5° (FWHM) depending on the pixel. The mounting and FoV of CENA and SWIM are shown in Fig. 1. Chandrayaan-1 was in a 100 km circular orbit till 18 May 2009; subsequently, the orbit was raised to 200 km. The orbital period at 100 km was around 118 min.

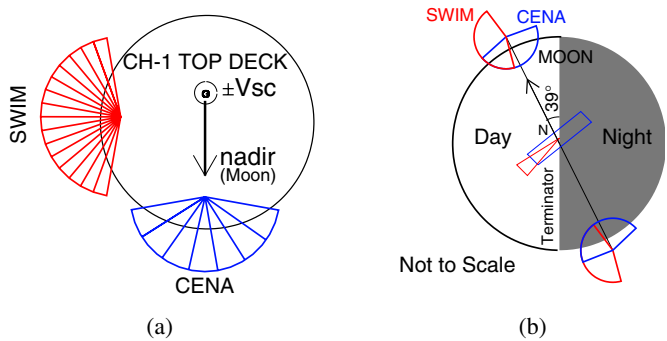


Fig. 1. (a) Mounting of CENA and SWIM on the Chandrayaan-1 along with their Field-of-View (FoV). CENA is nadir viewing towards Moon surface and the SWIM is mounted 90° to CENA such that few view directions of SWIM looks at the Moon surface. The arrows indicates the nadir direction and the spacecraft velocity vector. (b) The FoV of SWIM and CENA along with the orbital motion of Chandrayaan-1 for the day 15 February 2009 when the orbital plane of Chandrayaan-1 was at an angle of 39° with the day-night terminator.[42]

Table 1. Characteristics of CENA and SWIM.[40]

| Parameter | CENA | SWIM |
|---|---|---|
| Particle to measure | Neutrals | Ions |
| Energy range | 10 eV–3.2 keV | 10 eV–15 keV |
| Energy resolution | 50% | 7% |
| Mass range (amu) | 1–56 | 1–40 |
| Mass resolution | H, O, Na/Mg/Si/Al-group, K/Ca-group, Fe-group | $H^+$, $He^{++}$, $He^+$, $O^{++}$, $O^+$, >20 amu |
| Full field-of-view | 15° × 160° | 9° × 180° |
| Angular resolution | 9° × 25° (E > 50 eV) | 4.5° × 22.5° |
| Efficiency (%) | 0.01–1 | 0.1–5 |
| Sensor mass | 1977 g | 452 g |

The instrument parameters of CENA and SWIM are presented in Table 1.

## 3. Observations and Results

### 3.1. *Observation pertaining to ENAs*

#### 3.1.1. *ENAs backscattered from lunar surface*

SARA has observed energetic neutral hydrogen atoms (hydrogen ENAs) from the Moon surface.[1] The source of these ENAs are solar wind protons

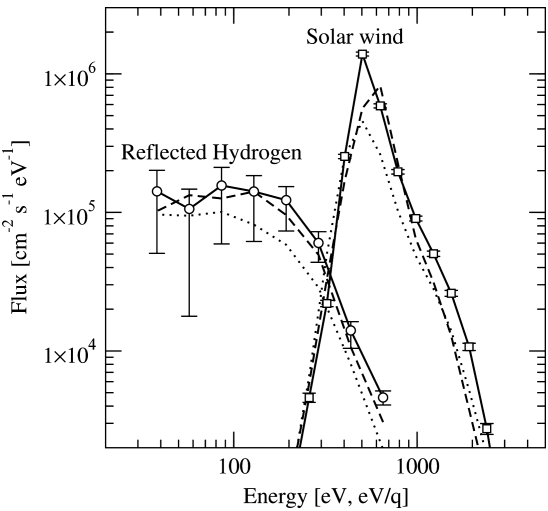


Fig. 2. Energy spectrum of solar wind and the ENAs scattered from lunar surface on 5 February 2009 for three orbits which are showed in solid line, dashed line and dotted line with dayside equator crossings at 05:22 UTC, 07.20 UTC, and 09:18 UTC, respectively. The dependence of the flux of scattered ENA on the incident solar wind flux is clearly visible from these spectra.[1]

which get neutralized in the interaction with the Moon surface and are scattered back to space. This is contrary to the earlier belief that the lunar surface completely absorbs the incident solar wind.[16,17] Most of the ENAs are found to have energy less than ∼50% of the incident solar wind energy. The energy spectrum of the hydrogen ENAs shown in Fig. 2 is broader than the incident solar wind protons. One of the mechanisms for the energy loss may be the multiple scattering process due to interaction with the lattice. The observations showed that about 20% of the incident solar wind flux is backscattered as ENAs from the lunar regolith (Fig. 3). The solar zenith angle (SZA) dependence of the flux of scattered ENAs could be seen in Fig. 3. The higher energy of the ENAs is indicative that they are indeed solar wind backscattered ENAs as opposed to the sputtered ENAs whose energies based on model calculations are expected to be much lower (around few eV).[18] The IBEX observations of lunar ENAs suggests that the solar wind backscatter efficiency is 10%[29,43] and the analysis of the energy spectra indicates that they are indeed backscattered ENAs and not sputtered particles.

The solar wind ions which are absorbed or implanted in the lunar regolith can get released to the lunar exosphere due to processes such as

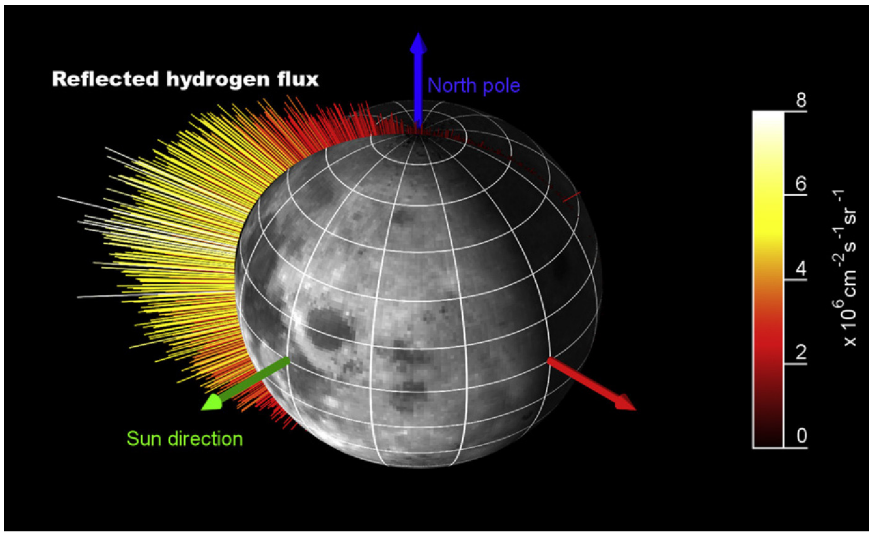


Fig. 3. Map of scattered energetic neutral hydrogen atoms as observed by SARA on 6 February 2009. The direction of Sun is indicated in the figure. The ENA signature was seen for three consecutive orbits and the orbital plane was at an angle of 39° with the day–night terminator plane. The gradient in grey-scale and length of the lines indicates the ENA flux. The small flux seen on night-side is due to instrument background. The variation of ENA flux with solar zenith angle is seen in the map. The lunar surface map is from Clementine image data.[1]

diffusion, solar wind sputtering, and micrometeorite impact vaporization. The significant energy loss of the observed ENAs compared to impinging solar wind is due to elastic and inelastic processes during surface–plasma interactions, and possibly other processes such as retarding of solar wind ions by a positive surface potential.

*Hodges*[44] has modeled the scattering of the solar wind from lunar surface using an inter-atom transport model for fast hydrogen in the surface layers of lunar soil grains and rocks. He had taken into account the rapid charge exchange neutralization of incident solar wind protons and also multiple encounters of free hydrogen with loosely packed soil grains. The modeled energy spectra compare well with CENA/SARA observations,[1] but the modeled scattering efficiency is higher by a factor of three compared to the SARA observation.

### 3.1.2. *Mini-magnetosphere observed in backscattered ENAs*

Although Moon does not possess a global magnetic field,[45,46] it is found to have regions of localized magnetic field called magnetic anomaly

regions.[10,14,47–49] There were speculations[12] that these small areas of locally strong magnetic field can create mini-magnetospheres that may deflect the solar wind in the same way that Earth's magnetosphere shields most of the planet from the solar wind. SARA has shown for the first time an existence of a mini-magnetosphere above the magnetic anomaly region using the backscattered ENAs.[2] The image of a lunar magnetic anomaly of strength ∼100 nT in the backscattered hydrogen ENAs for the Crisium antipode anomaly near the Gerasimovic crater is shown in Fig. 4. The image shows that a partial void of the solar wind, a mini-magnetosphere, is formed above the strong magnetic anomaly. Above the magnetic anomaly region, the flux of backscattered hydrogen ENAs was significantly lower than the surrounding areas indicating that the region was shielded from solar wind particles by a mini-magnetosphere.[2]

The spatial variation in the flux of backscattered hydrogen ENA shows a reduction of about 50% within the area of the mini-magnetosphere (inside dotted circle in Fig. 4a) compared to the surrounding ring shaped region of enhanced flux (dashed line) for ENAs in the 150–600 eV energy range. In the map for lower energies shown in Fig. 4b, it is seen that the large scale depletion in the neutral hydrogen flux above the magnetic anomaly is replaced by small scale fluctuations and the region of enhanced flux has become almost a filled circle, which are due in part to a low instrument count rate and may also reflect energy dependent angular scattering properties of regolith surfaces, with higher energy scatter products possibly being more specularly reflected than lower energy scatter products. The mini-magnetosphere is 360 km across at the surface and is surrounded by a 300 km thick circular region of enhanced plasma flux that results from the solar wind flowing around the mini-magnetosphere, for a magnetic anomaly of strength 100 nT at lunar surface.[2]

### 3.1.3. *Distribution of hydrogen ENAs backscattered from the Moon*

The angular distribution of the scattered ENAs was investigated by making use of the CENA observations.[50] Around 290,000 data points were used for the study so that almost full coverage of SZA, polar (0–90°), and azimuthal (0–360°) angles of scattering is achieved. The observation of hydrogen ENAs in the energy range 19–740 eV were considered. The observed angular scattering depends on the SZA (Fig. 5) such that as the SZA increases, more scattering takes place in the sunward direction than in the anti-sunward direction, which is contrary to what is expected

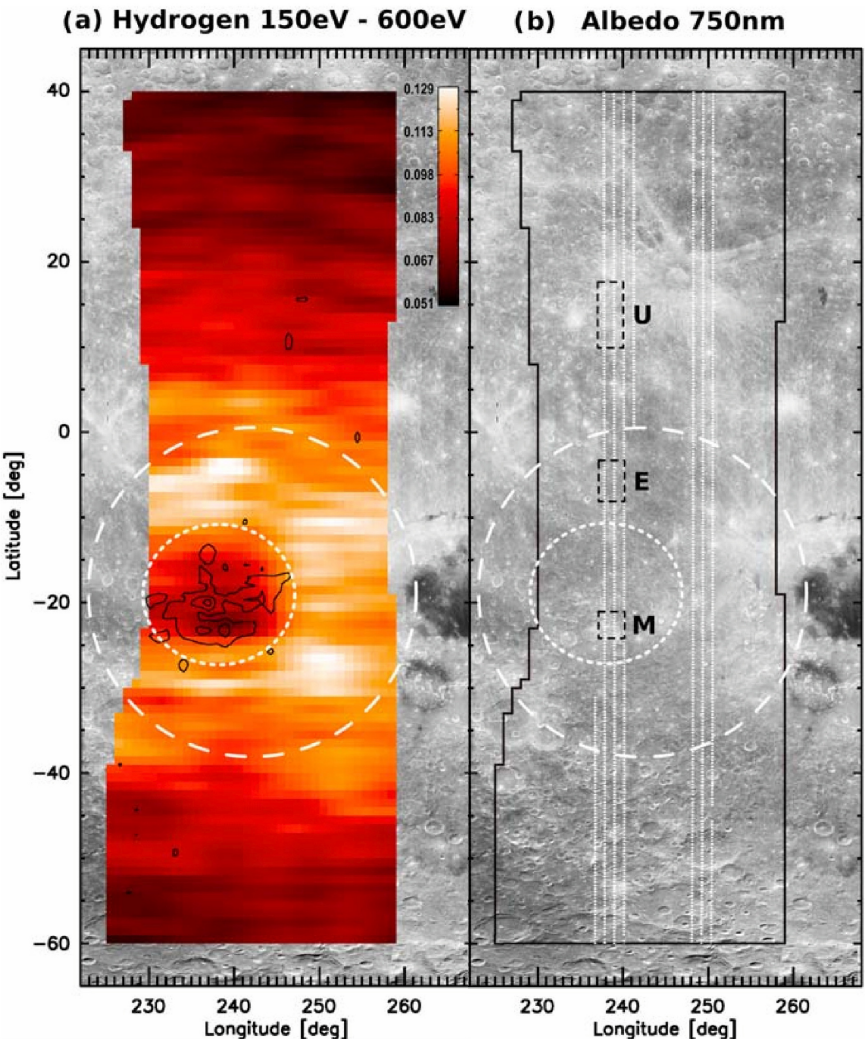


Fig. 4. The energetic neutral hydrogen flux from the surface over the magnetic anomaly near 22°S and 240°E on the lunar farside based on the observation on 17 June 2009 from 200 km altitude. The maps show a unit-less reflection coefficient: neutral hydrogen number flux integrated over the specified energy range divided by total solar wind number flux integrated over energy and multiplied by cosine of lunar latitude in the energy ranges (a) 150–600 eV (b) 30–100 eV. Black contours in the center show the magnetic field magnitude at 30 km altitude obtained from Lunar Prospector data, with lines for 5 nT, 15 nT, and 25 nT. The dotted circle represents the region of magnetic anomaly and the dashed circle represents the region just surrounding the anomaly. (c) Context image taken from the Clementine grey scale albedo map where the regions M, E and U indicate three sample regions inside the mini-magnetosphere, the enhanced flux region, and the undisturbed region, respectively.[2]

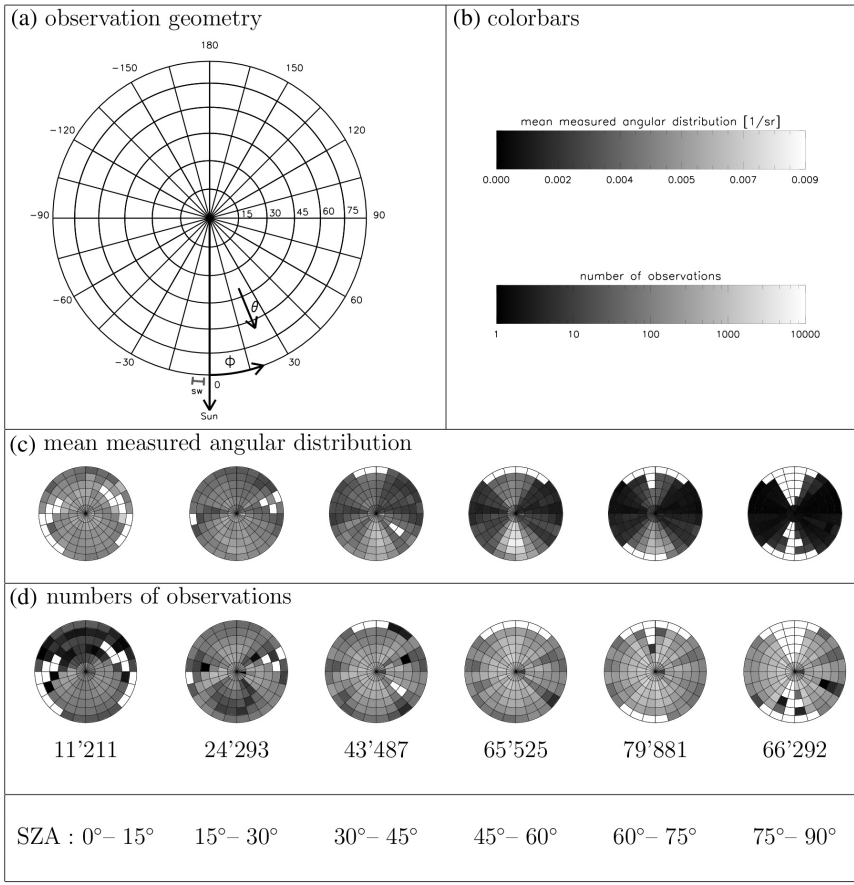


Fig. 5. The angular distribution of the scattered hydrogen ENA for 15° SZA intervals. Empty squares correspond to $(\theta, \phi)$ configurations for which we have no measurements. (a) Shows the coordinate system used for generating the maps shown in panels c and d. The arrow labeled "Sun" points in the sunward direction. For the sub-solar point (SZA = 0°) the arrow would be pointing out of the plane of the page along the normal, for a SZA of 90° the arrow lies in the page plane (depicted). (b) Contains the grey-scale bar, the first bar belongs to panel c, and the second bar belongs to panel d. (c) The measured angular distributions. (d) The number of observations.[50]

based on laboratory studies.[51] In addition, with the increase in SZA, the polar angle of scattering measured from the direction of surface normal also increases (shallower scattering). A mathematical expression which describes the observed angular scattering was derived as a function of SZA, polar, and azimuth angles of scattering.[50] This provides a useful way to represent the

scattering function for solar wind produced ENAs from a regolith covered non-magnetized bodies in the solar system.

### 3.2. *Observations pertaining to ions around the Moon*

The SWIM sensor of SARA has observed different populations of ions around Moon.[5] The energy-time spectra from the SWIM observations for two orbits on 25 January 2009 is shown in Fig. 6. It may be noted that a few viewing direction of SWIM directly faces the Moon surface (Fig. 1). The spectra is divided into three panels depending on the viewing direction in which the ions are observed, such as space, horizon, and surface viewing. The different ion populations are marked by letters A to E. The population A, which is observed in the space viewing directions, when SWIM was on dayside, are the solar wind protons which have energy around 500–600 eV/q. In the same viewing directions, SWIM has observed ion population B during dayside, which have an energy/charge almost twice that of solar wind $H^+$ energy/charge. These are the $He^{++}$ ions in the solar wind. The population C is seen in the surface viewing pixels of SWIM on the dayside which have lower count rate and broader energy compared to that of solar wind protons. This represents the solar wind protons which are scattered from the lunar surface. The population D which are seen mostly close to the horizon are

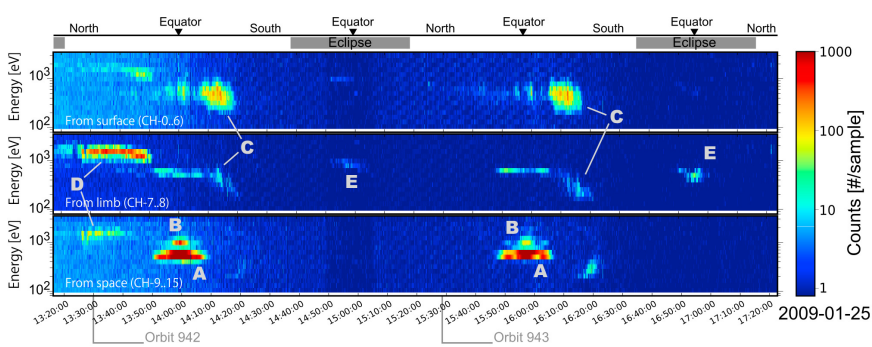


Fig. 6. The energy time spectra of ions observed by SWIM for two consecutive orbits on 25 January 2009. The bottom panels represent the observation from the view directions of SWIM which looks at space, the center panel represents data from the view directions towards the Moon limb, and the top panel represents observations from view directions which looks at Moon surface. The population marked A and B are the direct solar wind $H^+$ and $He^{++}$ ions, respectively. The population C is the solar wind $H^+$ reflected from Moon surface, D is the accelerated protons from population C, and E is the night side ions. The grey boxes on the top represents when Chandrayaan-1 was on lunar night side.[5]

the reflected ions which are the scattered solar wind protons picked up by the interplanetary magnetic field ($B_{sw}$) and accelerated by the solar wind convective electric field ($E_{sw}$), thereby gaining energy. The population E are the ions seen when Chandrayaan-1 was on the nightside (plasma wake) of Moon. This represents the ions in the near-lunar plasma wake, which are found by mass analysis to be mostly protons. Except the population D, all others are seen for both the orbits. The trajectory of population D depends on the orientation of IMF and the convective electric field ($E_{sw} = -V_{sw} \times B_{sw}$, where $V_{sw}$ is the solar wind velocity). The orientation of $B_{sw}$ was different for the two orbits. So the trajectories of the reflected ions were such that they were able to enter SWIM FoV in the first orbit and not in the second orbit due to the change in orientation of $B_{sw}$.[5]



3.2.1. *Deflection of solar wind protons over the magnetic anomalies*

As mentioned above, SWIM has measured the solar wind protons reflected from the lunar surface in the surface looking pixels. This has been observed by SWIM in almost all orbits of Chandrayaan-1. The SWIM observations of reflected protons were found to be highly correlated to the crustal magnetic field.[4] Figure 7 shows SWIM data where the spacecraft passes by a large region of magnetic anomalies. Reflected protons, with energies similar to the solar wind, are clearly observed when magnetic anomalies are within the instrument field of view. This indicates that the observed protons are actually solar wind protons that have been deflected over the magnetic anomalies.[4] A map of these deflected protons for the lunar far-side is shown in Fig. 8. It is notable that deflection can be observed even from small, isolated anomalies. The deflection ratio of solar wind protons integrated over the full far-side hemisphere is 1%, while over the magnetic anomaly regions alone it is around 10%, and over the strongest anomalies it reaches over 50% (see Fig. 9). Kaguya[32] has also reported the deflection of solar wind protons by the magnetic anomaly near the South Pole Aitken region with an efficiency of more than 10%.

3.2.2. *Ions in the near-lunar wake*

Significant proton fluxes were detected (cf. Fig. 6) by SWIM in the near-plasma wake region of the Moon. On 25 January 2009, when the protons moved along IMF in to the wake their energy was slightly higher than that of the solar wind protons. The protons were detected close to the lunar equatorial plane at a SZA of 140°, i.e. ∼50° behind the terminator at a

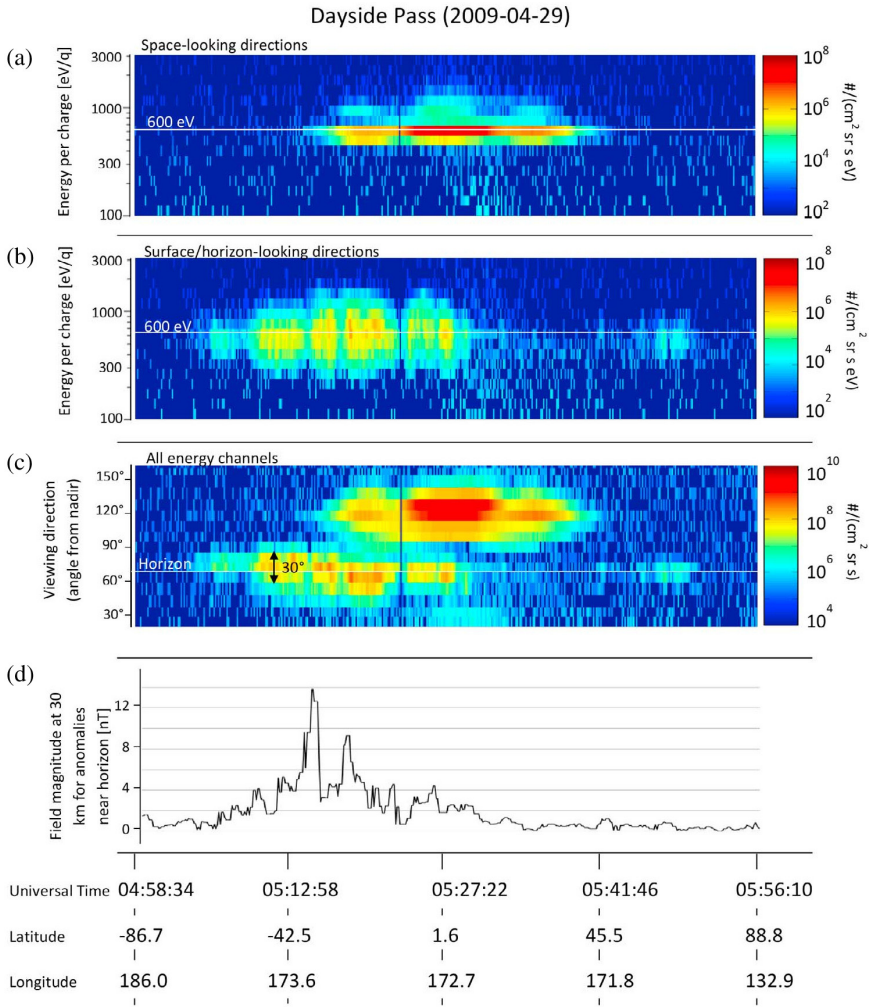


Fig. 7. SWIM-SARA observation during dayside pass of Chandrayaan-1 between 04:58 and 05:57 on 29 April 2009, over the Imbrium antipode magnetic anomalies. The top two panels represent the energy distribution of the ions with the differential flux summed over (a) five space-pointing directions (104–142° from nadir) and (b) five surface-pointing directions (44°–80° from nadir). (c) The direction distributions in angle from nadir, with the differential flux integrated over the 100 eV–3 keV energy range. (d) The strength of magnetic anomalies near the horizon is shown for reference. The strength is given in field magnitude at 30 km altitude based on model by Purucker (2008),[52] from Lunar Prospector data. Also shown is the time of observation as well as the selenographical coordinates.[4]

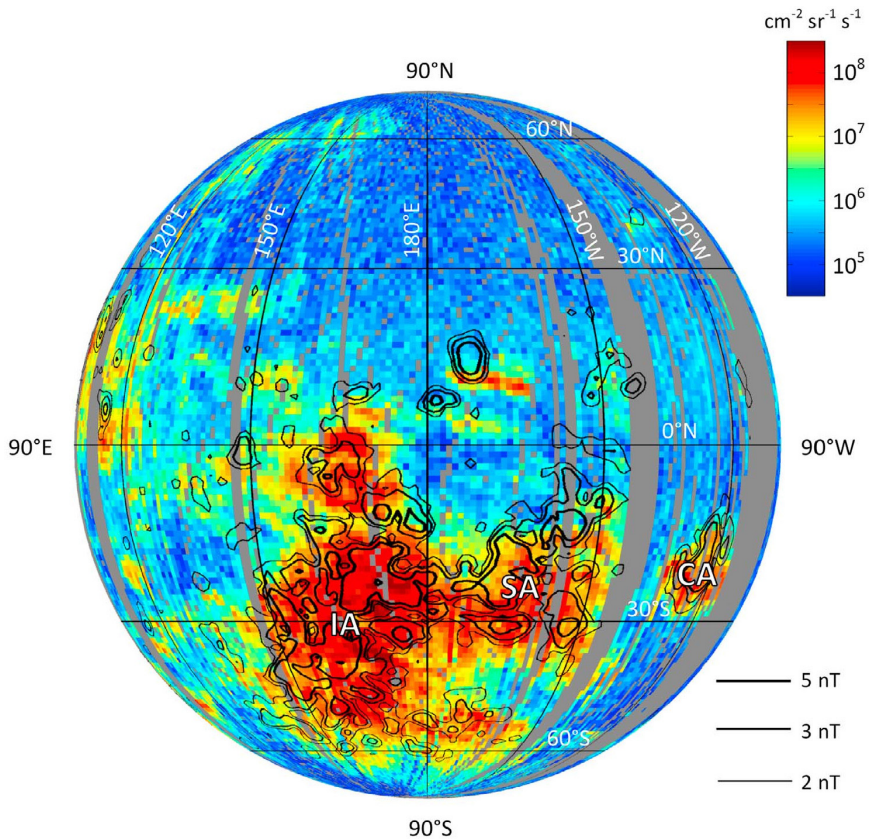


Fig. 8. The map of deflected solar wind protons observed in the 200 eV–1.7 keV energy range obtained by SWIM/SARA observations. The peak differential flux of protons is traced linearly to the surface of the Moon and binned to a 1° × 1° resolution spatial grid. Black contours show 2 nT, 3 nT, and 5 nT magnetic field strength at 30 km altitude in model by Purucker.[52] The large anomaly cluster at the Imbrium Antipode (IA), the Serenitatis Antipode (SA) and, the Crisium Antipode (CA) are marked in the figure.[4]

height of 100 km. The protons came from just above the local horizon, and moved along IMF in to the wake.[5] The comparison of the observed proton flux with the predictions of 1-D expansion of plasma into a vacuum showed that the observed velocity is higher than the velocity predicted by analytical models by a factor of two to three while the observed density is lower than the model value.[5]

As the solar wind is a magnetized plasma, the entry of solar wind ion in to the plasma wake is governed by the orientation of IMF. The protons in

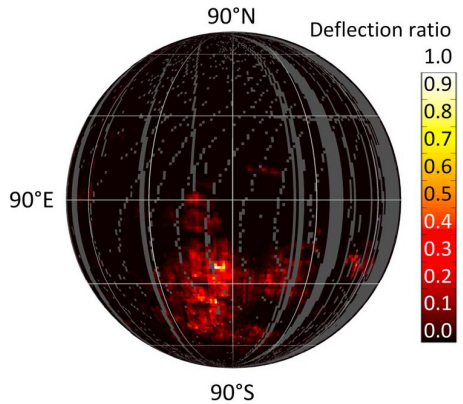


Fig. 9. Map of the ratio of the outflowing proton flux to the incident proton flux. The outgoing proton flux is calculated from SWIM data and inflowing proton flux is calculated from WIND data.[4]



the near-lunar wake have also been observed by Kaguya[33,34] and Chang'E,[35] where the protons entered the wake in a direction perpendicular to IMF. There are four possible mechanisms suggested for entry of ions in to the near-lunar plasma wake. Out of these, three mechanisms favor entry in a direction perpendicular to IMF, can be called as perpendicular entry,[33–35] and one mechanism favors entry of ions parallel to IMF[5] (parallel entry).

### 3.2.3. *The reflected ion trajectory: Modeling*

The protons reflected from the Moon surface will be influenced by the magnetic field carried by the solar wind (IMF) and the convective electric field ($E_{sw}$). For an IMF of 5 nT, the convective electric field is in the range 1.5–5.5 mV/m for a solar wind velocity ($V_{sw}$) in the range 300–700 km $s^{-1}$ (assuming $V_{sw}$ and IMF are perpendicular to each other). Thus, the protons could get accelerated by $E_{sw}$ and gyrate around IMF ($E \times B$ drift). These are surface reflected ions and seen as population D in Fig. 6.

Modeling the trajectory of these reflected ions (under Lorentz force) using a test particle approach, as well as hybrid model,[3] showed that the reflected solar wind protons affect the global plasma environment (Fig. 10). The results of the model is compared with observations. The broadening of the energy spectrum of reflected protons seen in the model result is consistent with the SARA observation. Comparing with Nozomi's ion observation revealed that the probable source of the non-thermal protons observed by Nozomi[53] in the lunar vicinity were the reflected protons.

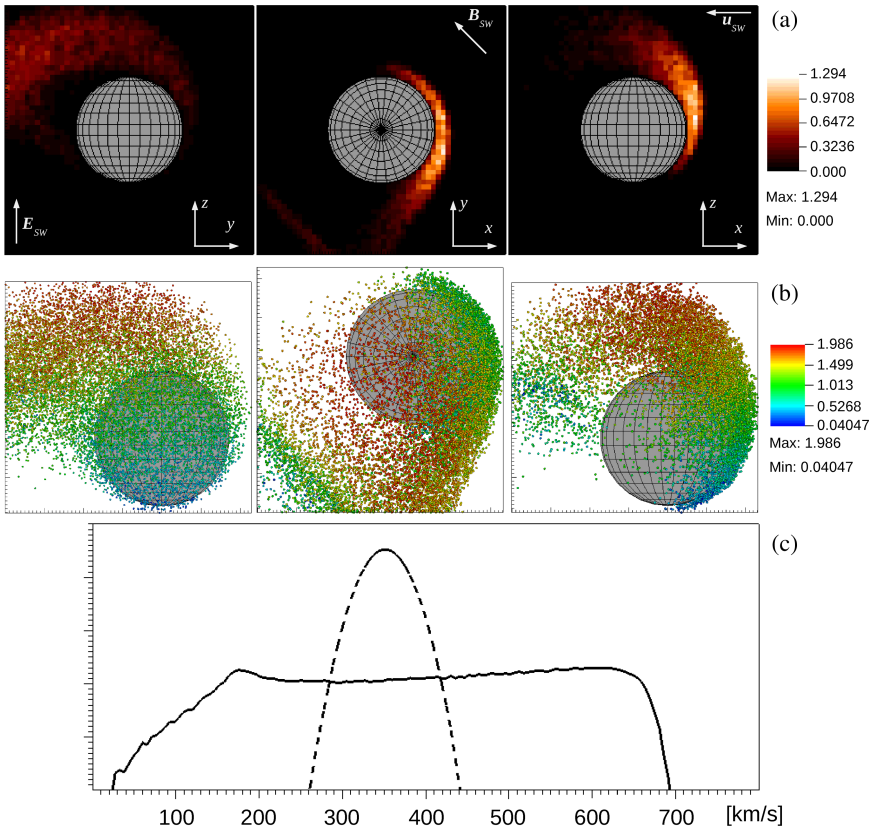


Fig. 10. The results of a run of the test particle simulation. The grey-scale shows the ratio of the magnitude of the yz component of the proton number flux (number density times average velocity) around the Moon, to the magnitude of the solar wind proton number flux. Here, 100% reflection ($f = 1$) of the precipitating protons is considered but this can be scaled for any other value of f. The left panel, middle panel and the right panel shows the cuts through the planes $x = 0$, $z = 0$, and $y = 0$, respectively.[3]

## 4. Discussion

The ENA scattering from Moon reduces the implantation of solar wind protons. The implantation of solar wind hydrogen and its subsequent bonding with oxygen in the regolith has been suggested as a potential candidate for the formation of $OH/H_2O$ on Moon surface.[54–56] Although laboratory simulations by Burke *et al.*[57] using solid samples of ilmenite ($FeTiO_3$) and anorthite ($CaAl_2Si_2O_8$) did not show evidence for this, the very recent laboratory simulations by Managadze *et al.*[58] by using olivine and $SiO_2$ powders, which is more representative of the regolith composition,

has indeed shown that the solar proton is a potential source of lunar $OH/H_2O$ molecules. The contradiction in the results are attributed to the use of solid surface by Burke *et al.*[57] than the powdered sample used by Managadze *et al.*[58] Thus, the 20% backscattering of solar wind protons as ENAs will affect the production of $OH/H_2O$ on Moon surface by reducing the implantation rate of hydrogen. The proton scattering from Moon surface as ions also affect the implantation of hydrogen, but the fraction is much lower (0.1–1%) compared to the ENA scattering. On the other hand, the proton scattering has implications on the lunar plasma environment.

The presence of the mini-magnetosphere causes deflection of solar wind around the magnetic anomaly region, resulting in net increase in the solar wind incident flux on the area surrounding the magnetic anomaly and decrease in the incident flux over the anomaly region. This correlates well with the Chandrayaan-1 Moon Mineralogy Mapper ($M^3$) analysis of the spectral features of swirls and off-swirls at Reiner Gamma, Gerasimovich, and Mare Ingenii regions.[59] The analysis indicated that the swirls are depleted in OH relative to their surrounding region, supporting the view that the magnetic anomalies deflect the solar wind away from the swirls and onto off-swirl surfaces. In addition to the effect of reduced OH production in magnetic anomaly regions, the deflection of solar wind protons affects the spectral properties[22] of the soil at the anomaly region compared to the neighboring regions. This can be associated with magnetic shielding of the surface and the accumulation of fine charged dust above the swirls owing to the electrostatic interaction between charged fine grained dust and the electric field generated due to the charge separation between electrons and protons in the solar wind at magnetic anomaly.[60,61] The maturation of the soil will be higher in the region adjacent to the anomaly due to increased flux of protons deflected from the swirls. Similar spectral studies of immature craters and surface soils both on and adjacent to the lunar swirls at Mare Ingenii region using the Clementine ultraviolet, visible and near infra-red cameras[23] had also supported this hypothesis. Blewett *et al.*[60] have done an extensive study of the spectral characteristics of swirls and found them to be similar to those of immature soil and also that their FeO content to be lesser than the surrounding region. Connecting it with the presence of magnetic anomaly, they suggest that the difference in composition could be due to either the magnetic shielding of solar wind or the accumulation of dust moving under the influence of the electric field induced by solar wind interaction with magnetic anomaly. Observations of the enhanced albedo of the Descartes C crater by Mini-RF (radio frequency) synthetic

aperture radar on the Lunar Reconnaissance Orbiter is also found to be related to its location within a magnetic anomaly, and hence supports an origin hypothesis that invokes interaction between the solar wind and the magnetic anomaly.[62] The absence of lunar-type swirls on Mercury based on Messenger flybys also suggest that models for the formation of lunar swirls invoking the interaction between solar wind and crustal magnetic anomalies are of prime importance.[63]

The protons scattered from lunar surface can directly affect the lunar plasma environment.[3] Recent observations have shown that they cause whistler waves on the dayside of Moon.[64] Their trajectories can lead to their entry to the nightside.[34,35] The protons in the near wake cause instabilities and results in wave generation.[65] The existence of ions in deep near-wake indicates that not only the processes which happen in the immediate downstream but also the ones on dayside play a role in determining the nature of dynamics in the immediate downstream. Thus, both the fluid nature (plasma expansion into vacuum)[5] and particle nature of the solar wind (scattered protons reaching the nightside) play their role in the near-wake plasma features. Observations using Lunar Prospector magnetometer have shown the presence of whistler waves above the magnetic anomaly regions due to the interaction of solar wind with magnetic anomaly.[66]

All these indicate that the interaction of supersonic plasma flow with a planetary body without an atmosphere and intrinsic magnetic field is yet to be fully understood. The manifestation of the angular distribution of backscattered ENAs to be different from the expectations based on laboratory studies points to the requirement of further investigation of the micro-physics of the solar wind interaction with the regolith-covered planetary body. These results apply not only to Moon but also to any regolith covered planetary body with almost no atmosphere and lack a global magnetic field, but can have localized magnetic fields. Hence, these processes are expected to happen on Mercury, asteroids, and Moons of the giant planets also. The backscattering of solar wind protons have been observed recently on Phobos,[67] the Moon of Mars, by the Mars Express.

## 5. Summary

With a neutral particle detector (CENA) and ion-mass analyzer (SWIM), the SARA experiment on Chandrayaan-1 has made several interesting observations. These include (1) scattering of solar wind protons as ENAs

from Moon surface,[1] (2) scattering of solar wind protons itself from Moon surface,[3] (3) mini-magnetosphere around the magnetic anomaly region using both the scattered ENAs[2] as well as solar wind protons deflected by the magnetic anomaly,[4] (4) reflected ions which are the scattered solar wind protons influenced by the solar wind convective electric field and interplanetary magnetic field,[3] and (5) protons in the near lunar plasma wake.[5] Based on SARA observations: (1) the angular distribution of backscattered ENAs has been modeled,[50] (2) a model to understand the influence of trajectories of reflected protons on the lunar plasma environment has been developed.[3]

The micro-physics underlying the interaction between the solar wind particles and the porous lunar regolith which results in the observed angular distribution of the scattered ENAs and the scattering of protons are areas for future investigation.



## References

1. M. Wieser, S. Barabash, Y. Futaana, M. Holmström, A. Bhardwaj, R. Sridharan, M. B. Dhanya, P. Wurz, A. Schaufelberger and K. Asamura, *Planet. Space Sci.* **57** (2009) 2132.
2. M. Wieser, S. Barabash, Y. Futaana, M. Holmström, A. Bhardwaj, R. Sridharan, M. B. Dhanya, P. Wurz, A. Schaufelberger and K. Asamura, *Geophys. Res. Lett.* **37** (2010) L015103.
3. M. Holmström, M. Wieser, S. Barabash, Y. Futaana and A. Bhardwaj, *J. Geophys. Res.* **115** (2010) A06206.
4. C. Lue, Y. Futaana, S. Barabash, M. Wieser, M. Holmström, A. Bhardwaj, M. B. Dhanya and P. Wurz, *Geophys. Res. Lett.* **38** (2011) L03202.
5. Y. Futaana, S. Barabash, M. Wieser, M. Holmström, A. Bhardwaj, M. B. Dhanya, R. Sridharan, P. Wurz, A. Schaufelberger and K. Asamura, *J. Geophys. Res.* **115** (2010b) A10248.
6. R. M. Killen and W.-H. Ip, *Rev. Geophys.* **37** (1999) 361.
7. S. A. Stern, *Rev. Geophys.* **37** (1999) 453.
8. R. Sridharan, S. Ahmed, T. P. Das, P. Sreelatha, P. Pradeepkumar, N. Naik and G. Supriya, *Planet. Space Sci.* **58** (2010a) 947.
9. R. Sridharan, S. Ahmed, T. P. Das, P. Sreelatha, P. Pradeepkumar, N. Naik and G. Supriya, *Planet. Space Sci.* **58** (2010b) 1567.
10. P. J. Coleman, B. R. Lichtenstein, C. T. Russell, L. R. Sharp and G. Schubert, *Geochem. Cosmochem. Acta* **36** (1972) 2271.
11. L. L. Hood and G. Schubert, *Science* **208** (1980) 49.
12. R. P. Lin, D. L. Mitchell, D. W. Curtis, K. A. Anderson, C. W. Carlson, J. McFadden, M. H. Acuña, L. L. Hood and A. Binder, *Science* **281** (1998) 1480.

13. L. L. Hood, A. Zakharian, J. Halekas, D. L. Mitchell, R. P. Lin, M. H. Acuña and A. B. Binder, *J. Geophys. Res.* **106** (2001) 27825.
14. J. S. Halekas, D. L. Mitchell, R. P. Lin, S. Frey, L. L. Hood, M. H. Acuña and A. B. Binder, *J. Geophys. Res.* **106** (2001) 27841.
15. N. C. Richmond, L. L. Hood, J. S. Halekas, D. L. Mitchell, R. P. Lin, M. Acuña and A. B. Binder, *Geophys. Res. Lett.* **30** (2003) 1395.
16. W. C. Feldman, D. J. Lawrence, R. C. Elphic, B. L. Barraclough, S. Maurice, I. Genetay and A. B. Binder, *J. Geophys. Res.* **105** (2000) 4175.
17. D. H. Crider and R. R. Vondrak, *Adv. Space Res.* **30** (2002) 1869.
18. P. Wurz, U. Rohner, J. A. Whitby, C. Kolbb, H. Lammer, P. Dobnikar and J. A. Martín-Fernández, *Icarus* **191** (2007) 486.
19. A. Milillo, S. Orsini, K. C. Hsieh, R. Baragiola, M. Fama, R. Johnson, A. Mura, C. Plainaki, M. Sarantos, T. A. Cassidy, E. D. Angelis, M. Desai, R. Goldstein, W. H. Ip, R. Killen and S. Livi, *J. Geophys. Res.* **116** (2011) A07229.
20. A. Bhardwaj, S. Barabash, Y. Futaana, Y. Kazama, K. Asamura, R. Sridharan, M. Holmström, P. Wurz and R. Lundin, *J. Earth Syst. Sci.* **114** (2005) 749.
21. Y. Futaana, S. Barabash, M. Holmström and A. Bhardwaj, *Planet Space Sci.* **54** (2006) 132.
22. C. M. Pieters, E. M. Fischer, O. Rode and A. Basu, *J. Geophys. Res.* **98** (1993) 20.
23. G. Y. Kramer, J. P. Combe, E. M. Harnett, B. R. Hawke, S. K. Noble, D. T. Blewett, T. B. McCord and T. A. Giguere, *J. Geophys. Res.* **116** (2011a) E04008.
24. K. W. Ogilvie, J. T. Steinberg, R. J. Fitzenreiter, C. J. Owen, A. J. Lazarus, W. M. Farrell and R. B. Torbert, *Geophys. Res. Lett.* **10** (1996) 1255.
25. E. F. Lyon, S. B. I-I and I. B. J, *J. Geophys. Res.* **72** (1967) 6113.
26. W. M. Farrell, M. L. Kaiser and J. T. Steinberg, *Geophys. Res. Lett.* **24** (1997) 1135.
27. S. D. Bale, C. J. Owen, J.-L. Bougeret, K. Goetz, P. J. Kellogg, R. P. Lin, R. Manning and S. J. Monson, *Geophys. Res. Lett.* **24** (1997) 1427.
28. J. S. Halekas, Y. Saito, G. T. Delory and W. M. Farrell, *Planet. Space. Sci.* (2010).
29. D. J. McComas, F. Allegrini, P. Bochsler, P. Frisch, H. O. Funsten, M. Gruntman, P. H. Janzen, H. Kuchareck, E. M. obius, D. B. Reisenfeld and N. A. Schwadron, *Geophys. Res. Lett.* **36** (2009) L12104.
30. Y. Saito, S. Yokota, T. Tanaka, K. Asamura, M. N. Nishino, M. Fujimoto, H. Tsunakawa, H. Shibuya, M. Matsushima, H. Shimizu, F. Takahashi, T. Mukai and T. Terasawa, *Geophys. Res. Lett.* **35** (2008) L24205.
31. S. Yokota, Y. Saito, K. Asamura, T. Tanaka, M. N. Nishino, H. Tsunakawa, H. Shibuya, M. Matsushima, H. Shimizu, F. Takahashi, M. Fujimoto, T. Mukai and T. Terasawa, *Geophys. Res. Lett.* **36** (2009) L11201.
32. Y. Saito, S. Yokota, K. Asamura, T. Tanaka, Y. M. N. Nishino, Y. Terakawa, M. Fujimoto, H. Hasegawa, H. Hayakawa, M. Hirahara, M. Hoshino,

S. Machida, T. Mukai, T. Nagai, T. Nagatsuma, T. Nakagawa, M. Nakamura, K. Oyama, E. Sagawa, S. Sasaki, K. Seki, I. Shinohara, T. T. Terasawa, H. Shibuya, M. Matsushima, H. Shimizu and F. Takahashi, *Space Sci. Rev.* **154** (2010) 265.
33. M. N. Nishino, K. Maezawa, M. Fujimoto, Y. Saito, S. Yokota, K. Asamura, T. Tanaka, H. Tsunakawa, M. Matsushima, F. Takahashi, T. Terasawa, H. Shibuya and H. Shimizu, *Geophys. Res. Lett.* **36** (2009a) L12108.
34. M. N. Nishino, M. Fujimoto, K. Maezawa, Y. Saito, S. Yokota, K. Asamura, T. Tanaka, H. Tsunakawa, M. Matsushima, F. Takahashi, T. Terasawa, H. Shibuya and H. Shimizu, *Geophys. Res. Lett.* **36** (2009b) L16103.
35. X.-D. Wang, W. Bian, J.-S. Wang, J.-J. Liu, Y.-L. Zou, H.-B. Zhang, C. Lu, J.-Z. Liu, W. Zuo, Y. Su, W.-B. Wen, M. Wang, Z.-Y. Ouyang and C.-L. Li, *Geophys. Res. Lett* **37** (2010) L07203.
36. S. Wiehle, F. Plaschke, U. Motschmann, K.-H. Glassmeier, H. U. Auster, V. Angelopoulos, J. Mueller, H. Kriegel, E. Georgescu, J. Halekas, D. G. Sibeck and J. P. McFadden, *Planet. Space Sci.* **59** (2011) 661.
37. D. McCann, S. Barabash, H. Nilsson and A. Bhardwaj, *Planet. Space Sci.* **55** (2007) 1190.
38. Y. Kazama, S. Barabash, A. Bhardwaj, K. Asamura, Y. Futaana, M. Holmström, R. Lundin, R. Sridharan and P. Wurz, *Adv. Space Res.* **37** (2006) 38.
39. Y. Kazama, S. Barabash, M. Wieser, K. Asamura and P. Wurz, *Planet. Space Sci.* **55** (2007) 1518.
40. S. Barabash, A. Bhardwaj, M. Wieser, R. Sridharan, T. Kurian, S. Varier, E. Vijayakunar, V. Abhirami, K. V. Raghavendra, S. V. Mohankumar, M. B. Dhanya, S. Thampi, K. Asamura, H. Andersson, Y. Futaana, M. Holmstrm, R. Lundin, J. Svensson, S. Karlsson, R. D. Piazza and P. Wurz, *Current Science* **96** (2009) 526.
41. A. Bhardwaj, M. Wieser, M. B. Dhanya, S. Barabash, Y. Futaana, M. Holmstrm, R. Sridharan, P. Wurz, A. Schaufelberger and K. Asamura, *Advances in Geosciences* **19** (2010) 151.
42. M. B. Dhanya, A. Bhardwaj, Y. Futaana, S. Barabash, M. Wieser, R. Sridharan, M. Holmström and P. Wurz, private communication.
43. D. Rodriguez, L. Saul, P. Wurz, S. Fuselier, H. Funsten, E. M. obius and D. McComas, *Planet. Space Sci.* **60** (2012) 297.
44. R. R. Hodges, *Geophys. Res. Lett.* **38** (2011) L06201.
45. S. S. Dolginov, E. G. Eroshenko, L. N. Zhuzgov and N. V. Pushkov, *Geomagn. Aeron. Engl. Transl.* **1** (1961) 18.
46. N. S. Ness and K. W. Behannon and C. S. Scearce and S. C. Cantarano, *J. Geophys. Res.* **72** (1967) 5769.
47. K. A. Anderson, R. P. Lin, R. E. McGuire and J. E. McCoy, *Space Sci. Inst.* **1** (1975) 439.
48. R. P. Lin, *Phys. Earth Planet. Int.* **20** (1979) 271.
49. D. L. Mitchell, J. S. Halekas, R. P. Lin, S. Frey, L. L. Hood, M. H. Acuña and A. Binder, *Icarus* **194** (2008) 401.

50. A. Schaufelberger, P. Wurz, S. Barabash, M. Wieser, Y. Futaana, M. Holmstrm, A. Bhardwaj, M. B. Dhanya, R. Sridharan and K. Asamura, *Geophys. Res. Lett.* **38** (2011) L22202.
51. H. Niehus, W. Heiland and E. Taglauer, *Surf. Sci. Rep.* **17** (1993) 213.
52. M. E. Purucker, *Icarus* **197** (2008) 19.
53. Y. Futaana, S. Machida, Y. Saito, A. Matsuoka and H. Hayakawa, *J. Geophys. Res.* **108** (2003) 1025.
54. C. M. Pieters, J. N. Goswami, R. N. Clark, M. Annadurai, J. Boardman, B. Buratti, J.-P. Combe, M. D. Dyar, R. Green, J. W. Head, C. Hibbitts, M. Hicks, P. Isaacson, R. Klima, G. Kramer, S. Kumar, E. Livo, S. Lundeen, E. Malaret, T. McCord, J. Mustard, J. Nettles, N. Petro, C. Runyon, M. Staid, J. Sunshine, L. A. Taylor, S. Tompkins and P. Varanasi, *Science* **326** (2009) 568.
55. J. M. Sunshine, T. L. Farnham, L. M. Feaga, O. Groussin, F. Merlin, R. E. Milliken and M. F. A'Hearn, *Science* **326** (2009) 565.
56. T. B. McCord, L. A. Taylor, J. P. Combe, G. Kramer, C. M. Pieters, J. M. Sunshine and R. N. Clark, *J. Geophys. Res.* **116** (2011) E00G05.
57. D. J. Burke, C. A. Dukes, J.-H. Kim, J. Shi, M. Famá and R. A. Baragiola, *Icarus* **211** (2011) 1082.
58. G. G. Managadze, V. T. Cherepin, Y. G. Shkuratov, V. N. Kolesnik and A. E. Chumikov, *Icarus* **215** (2011) 449.
59. G. Y. Kramer, S. Besse, D. Dhingra, J. Nettles, R. Klima, I. G. Bethell, R. N. Clark, J. P. Combe, J. W. H. III, L. A. Taylor, C. M. Pieters, J. Boardman and T. B. McCord, *J. Geophys. Res.* **116** (2011b) E00G18.
60. D. T. Blewett, E. I. Coman, B. R. Hawke, J. J. Gillis-Davis, M. E. Purucker and C. G. Hughes, *J. Geophys. Res.* **116** (2011) E02002.
61. I. Garrick-Bethell, J. W. H. III and C. M. Pieters, *Icarus* **212** (2011) 480.
62. C. D. Neish, D. T. Blewett, D. B. J. Bussey, S. J. Lawrence, M. Mechtley, B. J. Thomson and T. M.-R. team, *Icarus* **215** (2011) 186.
63. D. T. Blewett, B. W. Denevi, M. S. Robinson, C. M. Ernst, M. E. Purucker and S. C. Solomon, *Icarus* **209** (2010) 239.
64. T. Nakagawa, F. Takahashi, H. Tsunakawa, H. Shibuya, H. Shimizu and M. Matsushima, *Earth Planets Space* **63** (2011) 37.
65. M. N. Nishino, M. Fujimoto, Y. Saito, S. Yokota, Y. Kasahara, Y. Omura, Y. Goto, K. Hashimoto, A. Kumamoto, T. Ono, H. Tsunakawa, M. Matsushima, F. Takahashi, H. Shibuya, H. Shimizu and T. Terasawa, *Geophys. Res. Lett.* **37** (2010) L12106.
66. J. S. Halekas, D. A. Brain, D. L. Mitchell and R. P. Lin, *Geophys. Res. Lett.* **33** (2006).
67. Y. Futaana, S. Barabash, M. Holmström, A. Fedorov, H. Nilsson, R. Lundin, E. Dubinin and M. Fränz, *J. Geophys. Res.* **115** (2010a) A10213.